J. Fluid Mech. (2019), *vol.* 876, *pp.* 5–18.
doi:10.1017/jfm.2019.513

Evolution of similarity lengths in anisotropic magnetohydrodynamic turbulence

Riddhi Bandyopadhyay[1,2], William H. Matthaeus[1,2,†], Sean Oughton[3] and Minping Wan[4]

[1]Department of Physics and Astronomy, University of Delaware, Newark, DE 19716, USA

[2]Bartol Research Institute, University of Delaware, Newark, DE 19716, USA

[3]Department of Mathematics and Statistics, University of Waikato, Hamilton 3240, NZ

[4]Department of Mechanics and Aerospace Engineering, Southern University of Science and Technology, Shenzhen, Guangdong 518055, PR China

(Received 31 January 2019; revised 18 June 2019; accepted 19 June 2019)

In an earlier paper (Wan *et al.*, *J. Fluid Mech.*, vol. 697, 2012, pp. 296–315), the authors showed that a similarity solution for anisotropic incompressible three-dimensional magnetohydrodynamic (MHD) turbulence, in the presence of a uniform mean magnetic field $\boldsymbol{B}_0$, exists if the ratio of parallel to perpendicular (with respect to $\boldsymbol{B}_0$) similarity length scales remains constant in time. This conjecture appears to be a rather stringent constraint on the dynamics of decay of the energy-containing eddies in MHD turbulence. However, we show here, using direct numerical simulations, that this hypothesis is indeed satisfied in incompressible MHD turbulence. After an initial transient period, the ratio of parallel to perpendicular length scales fluctuates around a steady value during the decay of the eddies. We show further that a Taylor–Kármán-like similarity decay holds for MHD turbulence in the presence of a mean magnetic field. The effect of different parameters, including Reynolds number, mean field strength, and cross-helicity, on the nature of similarity decay is discussed.

Key words: homogeneous turbulence, MHD turbulence, turbulence theory

1. Introduction

Turbulence is a ubiquitous phenomenon that spans a broad range of temporal and spatial scales. In a turbulent system energy is transferred from large (or 'energy-containing') eddies to small eddies, ultimately resulting in production of internal energy or heat by dissipation. This process of energy cascade is observed in turbulent neutral fluids as well as turbulent plasmas. The rate of energy decay in a turbulent system is both an interesting problem (Kolmogorov 1941) and also an important practical one. In laminar flows the rate of energy loss is determined by the molecular viscosity of the fluid, but in a turbulent system the energy dissipation rate appears to become independent of viscosity and approach a non-zero value as the

† Email address for correspondence: whm@udel.edu

fluid becomes increasingly turbulent (Onsager 1949). Taylor (1938) gave an empirical expression for the energy decay rate of turbulent neutral fluids. This analytical expression can be obtained from the work of de Kármán & Howarth (1938) by assuming the preservation of the shape of the two-point velocity correlation function during turbulent decay (Dryden 1943).

Energy decay in plasmas is a more complicated problem. Magnetohydrodynamic (MHD) theory is the simplest extension of hydrodynamic turbulence theories to conducting fluids and the decay of energy-containing eddies in MHD turbulence has been the subject of various studies (e.g., Hossain *et al.* 1995, 1996; Linkmann *et al.* 2015; Linkmann, Berera & Goldstraw 2017). Note that the presence of an external mean magnetic field, $\boldsymbol{B}_0$, makes the problem of energy decay in MHD more complex because the mean-field introduces anisotropy in the system (Robinson & Rusbridge 1971; Montgomery & Turner 1981; Montgomery 1982; Shebalin, Matthaeus & Montgomery 1983; Oughton, Priest & Matthaeus 1994; Hossain *et al.* 1995).

Energy cascade through the MHD inertial scales is given by a Kolmogorov–Yaglom (Kolmogorov 1941; Monin & Yaglom 1975) third-order law extended to MHD (Politano & Pouquet 1998*a*,*b*). On average, the energy transfer rate associated with cascading of excitation from the large scales (determined by the von Kármán-type phenomenology) and the energy cascade rate associated with inertial range scales (given by the third-order law) are expected to be in agreement (Kolmogorov 1941; Batchelor 1953; Bandyopadhyay *et al.* 2018).

The problem of similarity decay in isotropic and anisotropic incompressible MHD turbulence is studied in detail by Wan *et al.* (2012), where it is shown that similarity solutions are possible in MHD. However, unlike the situation for isotropic neutral fluids, universality, even at asymptotically high Reynolds number, is not expected for MHD due to potential variation of other parameters such as magnetic Prandtl number, cross-helicity, magnetic helicity and Alfvén ratio. Thus one might anticipate that in MHD the conditions for obtaining similarity solutions are more restrictive. Indeed, Wan *et al.* (2012) shows, analytically, that a similarity solution for MHD fluid with a mean magnetic field is possible only if, during the similarity decay, the similarity length scale parallel to the mean field remains proportional to the similarity length scale perpendicular to the mean-field. As far as we are aware, whether the two length scales remain in constant proportion has not yet been tested in simulations or experiments. This motivates the present study. We will discuss results from a set of (spectral method) numerical MHD turbulence experiments that examine the dynamical behaviour of the ratio of the parallel and perpendicular correlation scales. This enables us to assess whether or not a similarity decay phase occurs in anisotropic three-dimensional (3-D) MHD in the presence of a mean magnetic field (Wan *et al.* 2012). The results confirm, perhaps surprisingly, that the required condition for similarity decay of anisotropic MHD can be satisfied.

2. Theory

In this section we briefly review the Wan *et al.* (2012) derivation of similarity decay phenomenology for anisotropic MHD with a mean magnetic field. As in that work, we take the mass density to be constant and set it to unity. We denote the fluctuating velocity and magnetic fields by $\boldsymbol{v}$ and $\boldsymbol{b}$, respectively. Without loss of generality, we take the mean magnetic field as $\boldsymbol{B}_0 = B_0\hat{\boldsymbol{z}}$. All magnetic fields are converted to Alfvén units. The equations of incompressible MHD can be written in terms of Elsasser variables for the fluctuations, $\boldsymbol{z}^{\pm} = \boldsymbol{v} \pm \boldsymbol{b}$, as

$$\frac{\partial \boldsymbol{z}^{\pm}}{\partial t} = -\boldsymbol{z}^{\mp} \cdot \boldsymbol{\nabla} \boldsymbol{z}^{\pm} \pm \boldsymbol{B}_0 \cdot \boldsymbol{\nabla} \boldsymbol{z}^{\pm} - \boldsymbol{\nabla} P + \nu \nabla^2 \boldsymbol{z}^{\pm}, \tag{2.1}$$

where P is the total (magnetic + kinetic) pressure, and ν is the viscosity, for simplicity assumed to be equal to the resistivity herein.

The second-order correlation tensors for the corresponding Elsasser fields are defined as

$$R_{ij}^{\pm}(\boldsymbol{r}, t) = \langle z_i^{\pm}(\boldsymbol{x}, t) z_j^{\pm}(\boldsymbol{x}+\boldsymbol{r}, t)\rangle, \tag{2.2}$$

where $\langle\cdots\rangle$ denotes an ensemble average. Using the MHD equations one can derive the following equation for the time evolution of the traced second-order correlation function

$$\frac{\partial}{\partial t} R_{ii}^{\pm}(\boldsymbol{r}, t) = -\frac{\partial}{\partial r_k}[\hat{Q}_k^{\pm}(\boldsymbol{r}, t) - \hat{Q}_k^{\pm}(-\boldsymbol{r}, t)] + 2\nu \frac{\partial^2 R_{ii}^{\pm}}{\partial r_k \partial r_k}. \tag{2.3}$$

Here

$$\hat{Q}_k^{\pm}(\boldsymbol{r}, t) = \langle z_k^{\mp}(\boldsymbol{x}+\boldsymbol{r}, t) z_i^{\pm}(\boldsymbol{x}, t) z_i^{\pm}(\boldsymbol{x}+\boldsymbol{r}, t)\rangle \tag{2.4}$$

is a triple correlation. It is interesting that the mean magnetic field $\boldsymbol{B}_0$ does not appear explicitly in (2.3), despite the well known fact that these correlation functions (and their Fourier transforms, the Elsasser energy spectra) do display anisotropy relative to $\boldsymbol{B}_0$. In fact, the first explicit appearance of a mean magnetic field in the correlation function hierarchy is in the equation for evolution of the third-order correlations (Wan *et al.* 2012; Oughton *et al.* 2013). Consequently, the dynamical influence of $\boldsymbol{B}_0$ is exerted on (2.3) through the structure of the third-order correlations. Therefore, the limit of large $\boldsymbol{B}_0$ that permits reduction to quasi-two-dimensional MHD must occur in those higher order equations, and not directly in (2.3).

A set of similarity solutions can be derived from these equations using a heuristic scaling argument, as shown by de Kármán & Howarth (1938) for hydrodynamic turbulence and generalized to MHD by Wan *et al.* (2012). Here, we outline the steps only for the case of anisotropic MHD decay in the presence of a mean magnetic field. It is well established that a mean magnetic field affects the dynamics of the dissipation rate in a turbulent system (e.g., Shebalin *et al.* 1983; Oughton *et al.* 1994; Bigot, Galtier & Politano 2008*a*,*b*). Without loss of generality, we allow for non-zero cross-helicity $H_c = \langle \boldsymbol{v} \cdot \boldsymbol{b}\rangle$. The zero cross-helicity case is recovered as a special solution.

Assuming the system to be axisymmetric with respect to the mean-field direction $\hat{\boldsymbol{z}}$, we write the second-order correlation functions in the form

$$R_{ii}^{\pm}(\boldsymbol{r}, t) = R_{ii}^{\pm}(r_\parallel, r_\perp, t), \tag{2.5}$$

where $r_\parallel = \boldsymbol{r}\cdot\hat{\boldsymbol{z}}$ and $r_\perp = |\boldsymbol{r} - r_\parallel\hat{\boldsymbol{z}}|$. Clearly, $r_\parallel$ and $r_\perp$ are equivalent to the height (z) and radial (s) coordinates in the usual cylindrical polar coordinate system (s, ϕ, z). Using the theory of axisymmetric tensors (Batchelor 1953; Politano, Gomez & Pouquet 2003), the triple correlations can be written as

$$\hat{Q}_k^{\pm}(\boldsymbol{r}, t) = A^{\pm}(r_\parallel, r_\perp, t)\hat{r}_k + C^{\pm}(r_\parallel, r_\perp, t)\hat{\boldsymbol{z}}, \tag{2.6}$$

$$\hat{Q}_k^{\pm}(-\boldsymbol{r}, t) = -A^{\pm}(-r_\parallel, r_\perp, t)\hat{r}_k + C^{\pm}(-r_\parallel, r_\perp, t)\hat{\boldsymbol{z}}. \tag{2.7}$$

Inserting expressions (2.6)–(2.7) into (2.3) yields

$$\partial_t R_{ii}^{\pm} = -\left(\frac{\partial A_2^{\pm}}{\partial r_\perp}\frac{r_\perp}{r} + \frac{\partial A_2^{\pm}}{\partial r_\parallel}\frac{r_\parallel}{r} + \frac{2A_2^{\pm}}{r} + \frac{\partial C_2^{\pm}}{\partial r_\parallel}\right) + 2\nu\left(\frac{\partial^2 R_{ii}^{\pm}}{\partial r_\perp^2} + \frac{1}{r_\perp}\frac{\partial R_{ii}^{+}}{\partial r_\perp} + \frac{\partial^2 R_{ii}^{\pm}}{\partial r_\parallel^2}\right), \tag{2.8}$$

where

$$A_2^{\pm}(r_\parallel, r_\perp, t) = A^{\pm}(r_\parallel, r_\perp, t) + A^{\pm}(-r_\parallel, r_\perp, t), \tag{2.9}$$

$$C_2^{\pm}(r_\parallel, r_\perp, t) = C^{\pm}(r_\parallel, r_\perp, t) - C^{\pm}(-r_\parallel, r_\perp, t), \tag{2.10}$$

with $A_2^{\pm}(-r_\parallel, r_\perp, t) = A_2^{\pm}(r_\parallel, r_\perp, t)$ and $C_2^{\pm}(-r_\parallel, r_\perp, t) = C_2^{\pm}(r_\parallel, r_\perp, t)$.

Following de Kármán & Howarth (1938) and Wan *et al.* (2012) we assume

$$R_{ii}^{+}(\boldsymbol{r}, t) = Z_+^2 f(\eta_\parallel, \eta_\perp), \tag{2.11}$$

$$A_2^{+}(\boldsymbol{r}, t) = Z_- Z_+^2 a(\eta_\parallel, \eta_\perp), \tag{2.12}$$

$$C_2^{+}(\boldsymbol{r}, t) = Z_- Z_+^2 c(\eta_\parallel, \eta_\perp). \tag{2.13}$$

introducing the normalized variables $\eta_\parallel = r_\parallel / L_\parallel^+(t)$ and $\eta_\perp = r_\perp / L_\perp^+(t)$, and the shorthand notation $Z_\pm^2 = R_{ii}^{\pm}(0, t) = \langle |z_\pm|^2 \rangle$. Using (2.11)–(2.13), in (2.8) we obtain

$$\begin{aligned}
&\left\{\frac{\mathrm{d}Z_+^2}{\mathrm{d}t}\right\}[f] - \left\{\frac{Z_+^2}{L_\parallel^+}\frac{\mathrm{d}L_\parallel^+}{\mathrm{d}t}\right\}\left[\frac{\partial f}{\partial \eta_\parallel}\eta_\parallel\right] - \left\{\frac{Z_+^2}{L_\perp^+}\frac{\mathrm{d}L_\perp^+}{\mathrm{d}t}\right\}\left[\frac{\partial f}{\partial \eta_\perp}\eta_\perp\right] \\
&\quad + \left\{\frac{Z_- Z_+^2}{L_\perp^+}\right\}\left[\frac{1}{\sqrt{\eta_\perp^2 + \gamma^2\eta_\parallel^2}}\left(\frac{\partial a}{\partial \eta_\perp}\eta_\perp + \frac{\partial a}{\partial \eta_\parallel}\eta_\parallel + 2a\right)\right] + \left\{\frac{Z_- Z_+^2}{L_\parallel^+}\right\}\left[\frac{\partial c}{\partial \eta_\parallel}\right] \\
&\quad - \left\{2\nu\frac{Z_+^2}{L_\parallel^{+2}}\right\}\left[\frac{\partial^2 f}{\partial {\eta_\parallel}^2}\right] - \left\{2\nu\frac{Z_+^2}{L_\perp^{+2}}\right\}\left[\frac{\partial f}{\partial \eta_\perp}\frac{1}{\eta_\perp}\frac{\partial^2 f}{\partial {\eta_\perp}^2}\right] = 0,
\end{aligned} \tag{2.14}$$

where $\gamma = L_\parallel^+ / L_\perp^+$. We assume here that the '+' and '−' variables are independent of each other. For ease of identification we have written all the terms that are explicitly dependent on time inside curly brackets: $\{\cdots\}$. Terms that do not explicitly depend on time are written inside square brackets: $[\cdots]$. There are two points to note here. First, because $\eta_\parallel$ and $\eta_\perp$ are functions of time, the square-bracketed terms will in general have implicit time dependence. Second, *a priori* one would expect the variable $\gamma = L_\parallel^+ / L_\perp^+$ to be time dependent. Thus, the claim that the square-bracketed terms lack explicit time dependence will only be true if γ is constant. The dynamical relevance of this constraint is the primary focus of this study.

As an aside, we note that this requirement for similarity solutions may not pertain to the asymptotic case of $\gamma^2\eta_\parallel^2 \gg \eta_\perp^2$, i.e., $r_\parallel^2 \gg r_\perp^2$. In this circumstance, the fourth term of (2.14) can be separated into a time-dependent part and a time-independent part, regardless of the behaviour of γ, in the asymptotic limit. Physically, this limit would be relevant to phenomena or structures that are strongly elongated along the parallel direction. A similarity solution might then exist without the need for $\gamma = \text{const}$.

Without pursuing the above mentioned limits here, and assuming that γ remains constant in time, we can gather all the terms inside curly brackets in (2.14) and set them proportional to each other. Proceeding accordingly, we can write

$$\frac{\mathrm{d}Z_+^2}{\mathrm{d}t} \propto \frac{Z_+^2}{L_\perp^+}\frac{\mathrm{d}L_\perp^+}{\mathrm{d}t} \propto \frac{Z_- Z_+^2}{L_\perp^+}, \tag{2.15}$$

so that

$$\frac{\mathrm{d}L_\perp^+}{\mathrm{d}t} = \beta^+ Z_-, \tag{2.16}$$

$$\frac{\mathrm{d}Z_+^2}{\mathrm{d}t} = -\alpha^+ \frac{Z_- Z_+^2}{L_\perp^+}, \tag{2.17}$$

where β^+ and α^+ are both positive time-independent constants. In deriving (2.16)–(2.17) we have ignored the terms containing the viscosity ν in (2.14), due to the assumption $\nu \ll 1$; i.e., high Reynolds number. The '$-$' versions of (2.14)–(2.17) are analogous.

Equations (2.16) and (2.17) can be heuristically derived from dimensional analysis and modelling (e.g., Dobrowolny, Mangeney & Veltri 1980; Hossain *et al.* 1995; Biskamp & Schwarz 2001). The derivation presented here and in Wan *et al.* (2012) highlights the underlying assumptions and limitations of these solutions. For example, the derivation relies on the assumption of similarity, i.e., that the two-point correlation function maintains its shape during the decay. Moreover, the requirement that γ needs to remain constant in time is manifested through this analysis.

Equations (2.16) and (2.17) are exactly satisfied if the solutions obey the conservation law

$$Z_+^{(2\beta^+/\alpha^+)} L_\perp^+ = \text{const.} \tag{2.18}$$

For the long time behaviour of Z_+ and $L_\perp^+$, one expects, on the basis of physical arguments for decaying turbulence (Matthaeus, Zank & Oughton 1996), that

$$\alpha^+ \geqslant \beta^+. \tag{2.19}$$

We now test these hypotheses using spectral simulations.

3. Simulations

To test the hypothesis that the Elsasser energies and correlation lengths of (unforced) MHD turbulence evolve according to von Kármán–Howarth similarity decay laws – (2.16)–(2.17) and their 'minus' partners – and which also requires that the ratio of the parallel and perpendicular characteristic lengths does not change in time, we carry out a set of incompressible MHD simulations with a mean magnetic field, $B_0\hat{z}$.

All runs are initialized with kinetic and magnetic spectra proportional to $1/[1 + (k/k_0)^{11/3}]$, with $k_0 = 4$ and only the Fourier modes within the band $1 \leqslant k \leqslant 15$ excited. The initial total energy is always normalized to one. Correlation lengths are small compared to the total box length for all runs. Table 1 contains a summary of the simulation parameters used for this study. Although we are here mainly concerned with anisotropy induced by a mean magnetic field, for context we also include results from an isotropic simulation that lacks a global mean field (run 11).

We numerically solve (2.1) in a periodic box using a pseudo-spectral solver without any external forcing. All the variables are expanded in a Fourier basis with transfer between real space and Fourier space performed using a fast Fourier transform. We use the second-order Runge–Kutta scheme for time-stepping, and the 2/3 rule for dealiasing. To ensure accuracy of the dissipation rates and spectra we require that $k_{max}\zeta > 1$ for all simulations (Donzis, Yeung & Sreenivasan 2008; Wan *et al.* 2010). Here k_{max} is the maximum resolved wavenumber and ζ is the Kolmogorov dissipation length scale.

For strong mean field, the simulations can be performed in non-cubic boxes, provided the parallel cascade (in addition to the perpendicular cascade) is well resolved (Oughton, Dmitruk & Matthaeus 2004). For a well-resolved case, a non-cubic simulation domain is not expected to modify the dynamics in incompressible MHD (Bigot *et al.* 2008*b*). We employ a cubic periodic box for all runs discussed herein.

Simulation	N^3	B_0	ν	σ_c	r_A	dt
Run 0	256^3	0.5	0.002	0	1.0	0.001
Run 1	256^3	1	0.002	0	1.0	0.001
Run 2	256^3	1	0.002	0.5	1.0	0.001
Run 3	256^3	1	0.002	0	0.5	0.001
Run 4	256^3	2	0.002	0	1.0	0.0005
Run 5	256^3	3	0.002	0	1.0	0.0004
Run 6	256^3	2	0.002	−0.5	1.0	0.0005
Run 7	256^3	4	0.002	0	1.0	0.00025
Run 8	256^3	2	0.002	0	2.0	0.0005
Run 9	256^3	2	0.002	0.8	2.0	0.0005
Run 10	512^3	1	0.0005	0	1.0	0.0005
Run 11	256^3	0	0.002	0.5	1.0	0.0005

TABLE 1. Simulation parameters for spectral simulations: grid size N^3, the mean magnetic field strength B_0, viscosity ν, initial normalized cross-helicity $\sigma_c = 2H_c/E$, initial Alfvén ratio $r_A = E_v/E_b$, time step dt.

4. Results

To study the decay dynamics of the energy-containing eddies we compute, at each time step, the 'Elsasser energies' Z_+^2 and Z_-^2 and their characteristic lengths along each Cartesian coordinate direction. The latter are calculated from the two-point correlation functions (see (2.2)) as

$$L_x^{\pm} = \frac{1}{Z_{\pm}^2} \int_0^{\infty} R^{\pm}(r, 0, 0)\, \mathrm{d}r, \tag{4.1}$$

and similarly for the y and z components. Here, $R^{\pm} = R_{ii}^{\pm}$ are the trace of the correlation tensors. In Fourier space, we can equivalently define the length scales as

$$L_x^{\pm} = \frac{\pi}{Z_{\pm}^2} \sum_{k_y, k_z} |\boldsymbol{z}^{\pm}(k_x = 0, k_y, k_z)|^2. \tag{4.2}$$

So, the length scales ($L_x^{\pm}$) are proportional to the reduced spectrum evaluated at zero wavenumber: $E_x^{red}(k_x = 0)$. We define

$$L_{\parallel}^{\pm} = L_z^{\pm}, \tag{4.3}$$

$$L_{\perp}^{\pm} = \sqrt{\frac{(L_x^{\pm})^2 + (L_y^{\pm})^2}{2}}. \tag{4.4}$$

The factor of $1/2$ in the definition of $L_{\perp}^{\pm}$ is used because there are two independent components in the perpendicular plane (e.g., Oughton & Matthaeus 2005). With this definition we usefully have $L_{\perp} \approx L_{\parallel}$ for the isotropic case, when $L_x \approx L_y \approx L_z$.

Figure 1 shows the time histories of the total fluctuation energy E (magnetic + kinetic), Elsasser energies $Z_{\pm}^2$, mean energy dissipation rate $\epsilon = \nu\langle j^2 + \omega^2\rangle$ and fluid Reynolds number Re for all the runs in table 1. Note that these quantities are associated with the fluctuations and, in particular, the calculation of Elsasser variables, their energies, and the total fluctuation energy does not include the contribution from

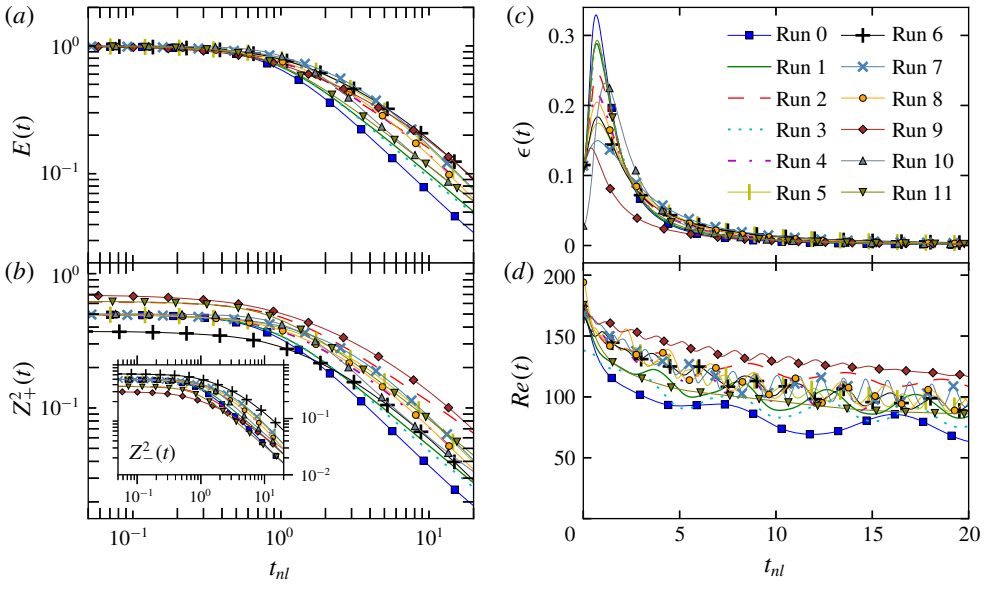

FIGURE 1. (Colour online) Time history of (*a*) the total fluctuation energy E, (*b*) the Elsasser energies $Z^2_{\pm}$ with '$-$' variables shown in the inset, (*c*) the mean energy dissipation rate $\epsilon = \nu\langle j^2 + \omega^2\rangle$, and (*d*) fluid Reynolds number Re for the runs listed in table 1. All quantities are defined in the text.

the mean magnetic field, $\boldsymbol{B}_0$. Here, $\boldsymbol{\omega} = \boldsymbol{\nabla} \times \boldsymbol{v}$ is the vorticity and $\boldsymbol{j} = \boldsymbol{\nabla} \times \boldsymbol{b}$ is the current density. The time axis is plotted in units of the initial nonlinear time or 'eddy turnover' time, $t_{nl} = t/\tau_{nl}$. We employ the following definition for the initial eddy turnover time

$$\tau_{nl} = \frac{[L^+(0) + L^-(0)]/2}{\sqrt{Z^2_+(0) + Z^2_-(0)}}, \tag{4.5}$$

where $L^{\pm}(0)$ are the initial correlation lengths, and

$$L^{\pm}(t) = \frac{\pi}{Z^2_{\pm}(t)} \sum_{\boldsymbol{k}} \frac{|z^{\pm}(\boldsymbol{k}, t)|^2}{|\boldsymbol{k}|}. \tag{4.6}$$

These are straightforward MHD generalisations of the classical definition of the correlation length or integral scale (Batchelor 1953; Linkmann *et al.* 2015; Bandyopadhyay *et al.* 2018*b*)

$$L_{int} = \frac{\pi}{E^v} \sum_{\boldsymbol{k}} \frac{E^v(\boldsymbol{k})}{|\boldsymbol{k}|}. \tag{4.7}$$

Note that we do not recover the directional length scales of (4.1), (4.2) by simply replacing $\boldsymbol{k}$ with k_x in (4.6). The fluid Reynolds number is defined as $Re = v' L_{int}/\nu$, where v' denotes the (average) component root mean square speed with $E^v = 3(v')^2/2$. Here, $E^v(\boldsymbol{k})$ is the modal kinetic energy spectrum and E^v is the total kinetic energy.

Panels (*a*) and (*b*) of figure 1 indicate that, for all runs considered, a power law (in time) is a reasonable approximation to the decay of both the total fluctuation energy

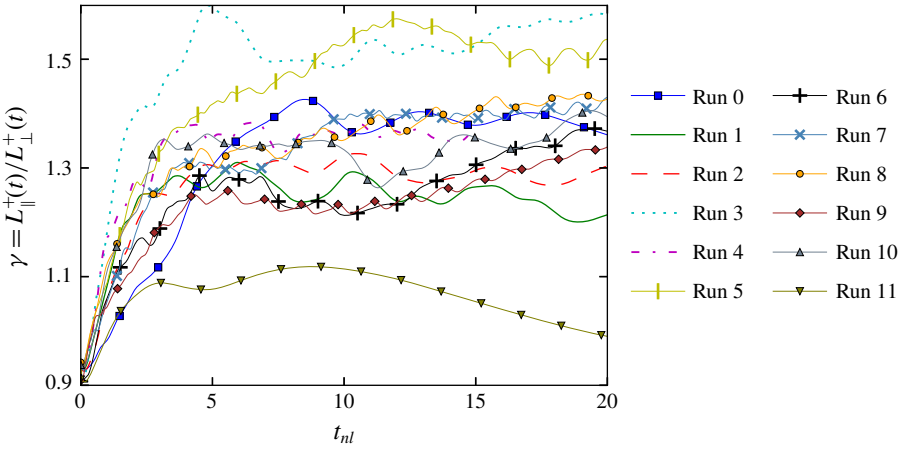

FIGURE 2. (Colour online) Time evolution of the ratio of parallel to perpendicular correlation lengths, $\gamma = L_\parallel^+/L_\perp^+$, for the runs of table 1.

and the Elsasser energies, after a few nonlinear times. This behaviour is expected for von Kármán–Howarth similarity decay (Matthaeus *et al.* 1996). Not all runs have the identical power-law slope and a full explanation for these slight differences is yet to be obtained. However, it is clear that the decay is (approximately) self-similar at these later times. During these $t \gtrsim 5\tau_{nl}$ periods the dissipation rates are much smaller than the peak values but are also only slowly decreasing; the Reynolds numbers are also slowly decreasing (with oscillations).

Figure 2 illustrates the time history of the ratio of the parallel to perpendicular length scales $\gamma = L_\parallel^+/L_\perp^+$, corresponding to the '+' Elsasser variable. It is evident that after an initial transient period, the ratio of the two length scales typically saturates to an approximately steady value, with fluctuations around those values.

A closer inspection of figures 1 and 2 reveals that the dissipation rate reaches its maximum near unit nonlinear time. However, γ values saturate at a somewhat later time $t_{nl} \sim 2$–5. This behaviour can probably be explained by noting that modifying the very large length scales takes a long time. The correlation lengths may become steady after the lowest wavenumber part of the spectrum is well populated. Since dissipation involves high wavenumber regions of the spectrum, where the characteristic time scales are much faster than those of the energy-containing eddies, it is perhaps not surprising that the dissipation rate peaks before γ saturates.

Although γ attains different values for different simulation sets, figure 2 indicates that for all cases γ remains approximately stationary for many nonlinear times. Furthermore, for the non-zero mean-field cases, $L_\parallel^+$ is always greater than $L_\perp^+$, indicating that the correlation lengths along the mean-field are longer than those perpendicular to it, due to the cascade preferentially transferring energy in the perpendicular directions (Shebalin *et al.* 1983; Grappin 1986; Matthaeus, Goldstein & Roberts 1990; Oughton *et al.* 1994; Goldreich & Sridhar 1995; Teaca *et al.* 2009).

Figure 2 contains the main results of this paper. (Plots for $\gamma^- = L_\parallel^-/L_\perp^-$, not shown, are completely analogous.) Having established that the ratio of parallel to perpendicular length scales remain (roughly) constant in time, we proceed to examine whether the proposed von Kármán similarity decay is satisfied for MHD fluids in the presence of a global magnetic field. In figure 3, we show the two 'von Kármán

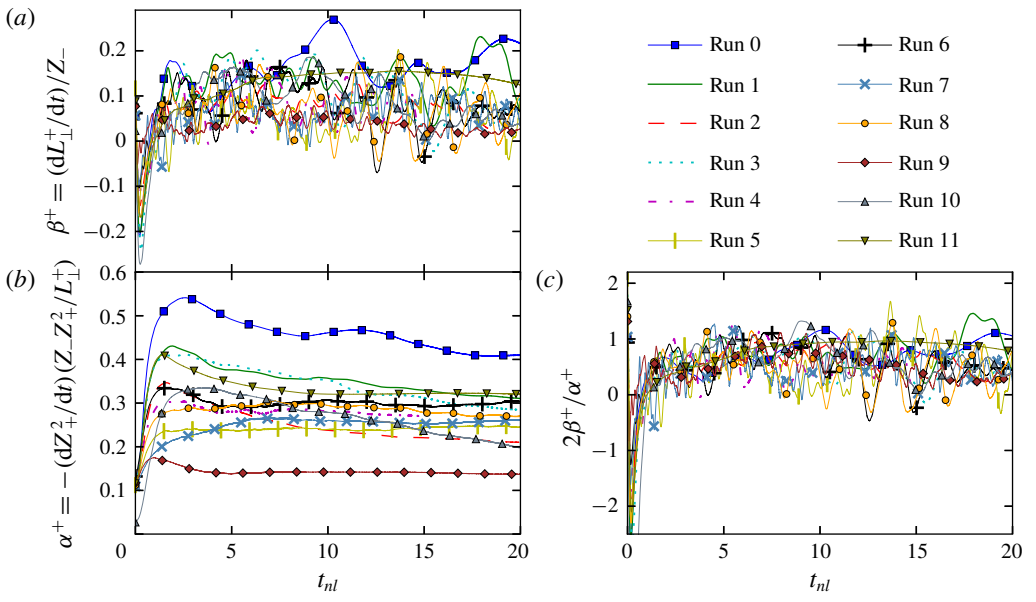

FIGURE 3. (Colour online) Time evolution of the two von Kármán constants: (*a*) $\beta^+ = (\mathrm{d}L_\perp^+/\mathrm{d}t)/Z_-$. (*b*) $\alpha^+ = -(\mathrm{d}Z_+^2/\mathrm{d}t)(Z_-Z_+^2/L_\perp^+)$, and (*c*) twice the ratio of the two constants, $2\beta^+/\alpha^+$, associated with the family of conservation laws, equation (2.18).

constants' α^+ and β^+, corresponding to the '+' Elsasser variables, as functions of time. If the similarity decay hypothesis is indeed satisfied, these two quantities should maintain constant values in time. Figure 3(*a*) shows the rate of change of perpendicular length scale $L_\perp^+$ normalized to Z_-, which, if the decay obeys a similarity solution is a constant, β^+. Panel (*b*) plots the (negative) normalized rate of change of Z_+^2 as a function of time; again, if the decay obeys a similarity this will be a constant, α^+. A central difference scheme is used to evaluate the time derivatives. It is clear from the two panels of figure 3 that the similarity decay hypothesis, as proposed in Wan *et al.* (2012), is well supported by the simulation results presented here.

Recall also, from (2.18), that the conserved quantity associated with the self-similar decay depends on the ratio $2\beta^+/\alpha^+$. This ratio is displayed in panel (*c*) of figure 3 where it can be seen that it attains a steady-state value of somewhat less than unity, after an initial adjustment phase. From Dryden (1943) and von Kármán & Lin (1949) self-similar decay for all scales requires $\alpha^\pm = \beta^\pm$. This situation corresponds to the case of decay with constant turbulent viscosity, $Z^\pm L^\pm = \text{const.}$, or equivalently decay at constant Reynolds number. Clearly, this is not satisfied rigorously in the simulations presented here. Further, the plotted values of $2\beta^+/\alpha^+$ appear to eliminate the possibility of similarity decay with $(Z^\pm)^2 L^\pm = \text{const.}$, physically corresponding to the case of constant area under the correlation function. Although only the '+' Elsasser variables are shown here, the results are similar for the '−' Elsasser variables. As an aside we note that applications of MHD decay phenomenologies within studies of the transport of solar wind fluctuations (e.g., Matthaeus *et al.* (1996), Zank, Matthaeus & Smith (1996), and many subsequent papers) have previously employed both the $\beta/\alpha = 1$ and the $2\beta/\alpha = 1$ conditions.

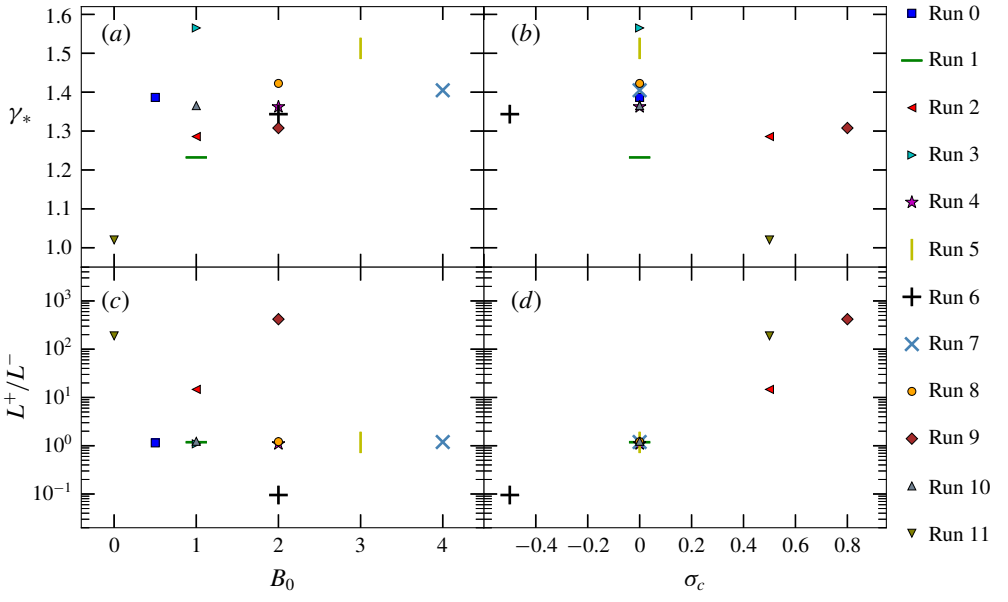

FIGURE 4. (Colour online) Variation of the asymptotic values of $\gamma = L_\parallel^+/L_\perp^+$ with (*a*) mean-magnetic-field strength B_0 and (*b*) the normalized cross-helicity σ_c, for the runs of table 1. Panels (*c*) and (*d*) plot the variation of the ratio L^+/L^- with B_0 and σ_c, respectively.

Next, we briefly discuss the effect of anisotropy due to the mean magnetic field strength B_0 and/or the cross-helicity strength. Of particular interest here is the variation of $\gamma = L_\parallel^+/L_\perp^+$ with B_0 and with the magnitude of the initial normalized cross-helicity σ_c. Figure 4 shows the asymptotic values of γ for all the runs. These asymptotic values, denoted γ_*, are obtained by averaging γ over the final five nonlinear times for each run. Within the limited parameter range scan of B_0 and σ_c covered by the simulations presented here, it appears that γ_* initially increases with B_0 but the effect then saturates for higher values of B_0. This behaviour is expected since the mean-field-induced anisotropy renders the system approximately two-dimensional; i.e., $L_\parallel > L_\perp$. On the other hand, from panel (*b*) of figure 4, no clear scaling can be deduced between γ_* and σ_c.

A related quantity of interest is the ratio of the length scales corresponding to the '+' and '−' Elsasser variables. Figure 4(*c*,*d*) illustrate the variation of the ratio L^+/L^-. Again, the reported values are the temporal averages over the final five nonlinear time units. Here, we see that there is no evident scaling with the mean-field strength B_0. However, panel (*d*) exhibits a rough increasing scaling of L^+/L^- with σ_c. This result is consistent with the explanation provided by Matthaeus, Goldstein & Montgomery (1983) and Ghosh, Matthaeus & Montgomery (1988), who argue that for high cross-helicity (say, positive), one of the Elsasser fields (z_-) is weak and it is almost passively advected towards high wavenumber by the dominant Elsasser field (z_+). This kind of tendency would result in dissimilar values of the two Elsasser field length scales ($L^+ \gg L^-$). From figure 4, the zero cross-helicity runs, run 0, 1, 3, 4, 5, 7, 8, 10, maintain $L^+/L^- \approx 1$. The positive cross-helicity runs, run 2, 9, 11, show $L^+/L^- > 1$, with increasing value of L^+/L^- as σ_c increases. Run 6 has $\sigma_c < 0$ and consequently $L^+/L^- < 1$ for this case.

5. Discussion

We have examined the validity of a von Kármán–Howarth-like similarity decay phase in anisotropic 3-D MHD in the presence of an externally supported mean magnetic field ($\boldsymbol{B}_0$), as derived in Wan *et al.* (2012). An analytic result is that a similarity decay phase is only followed in an MHD fluid (with a $\boldsymbol{B}_0$) if the ratio of the parallel to perpendicular characteristic length scales, $\gamma = L_{\parallel}^{+}/L_{\perp}^{+}$, remains constant in time. Using numerical simulations, performed with a range of different parameters, we find that the ratio of parallel to perpendicular length scales does indeed maintain an approximately steady value during the decay of the MHD turbulence, after an initial build-up phase. This result provides substantial support for the occurrence of similarity decay of energy in MHD turbulence with a mean-field.

Additionally, since the ratio of the parallel and perpendicular length scales maintains a constant value this implies that only one of the length scales evolves independently. This has useful consequences for global turbulence-based modelling of the solar wind and other astrophysical plasmas. Often in such models a von Kármán-like phenomenology is invoked (e.g., Breech *et al.* 2008; Oughton *et al.* 2011; Usmanov, Goldstein & Matthaeus 2014). If the parallel and perpendicular lengths maintain a constant proportion in the solar wind, it may be sufficient to evolve the length scale along only one direction, simplifying the calculations and possibly making the computations less expensive.

The results presented in this paper are important for understanding heating and acceleration of space plasmas such as the solar corona, solar wind and magnetospheric plasmas. The conclusions should also be useful for understanding and modelling the role of turbulence in the evolution and dynamics of astrophysical plasmas and laboratory plasmas.

We note that although the runs have the same initial conditions, after a few nonlinear times they evolve independently to distinct states. Therefore, we suggest that the result, that $L_{\parallel}/L_{\perp}$ maintains a steady value, does not depend on the large-scale eddies being of the same form in the parallel and perpendicular directions.

The applicability of the theory for modest Reynolds number warrants some discussion. To arrive at (2.16) and (2.17), we neglect the two terms proportional to ν in (2.14). This step can be justified by a simple calculation to estimate the order of magnitude of the neglected terms compared to the retained terms in (2.14). Let us compare the two terms $\{\mathrm{d}Z_{+}^{2}/\mathrm{d}t\}[f]$ and $\{2\nu Z_{+}^{2}/L_{\parallel}^{+2}\}[\partial^2 f/\partial\eta_{\parallel}^{2}]$. For simplicity, we ignore the notations $\parallel$, $\perp$, $\pm$, etc., and assume $f \sim \exp(-\eta)$. Then, we can compare the two terms as

$$\frac{\mathrm{d}Z^2}{\mathrm{d}t} : \nu\frac{Z^2}{L^2}. \tag{5.1}$$

For a consistency check, if we insert the desired solution, $\mathrm{d}Z^2/\mathrm{d}t \sim Z^3/L$, on the left-hand side we obtain

$$\frac{Z^3}{L} : \nu\frac{Z^2}{L^2}. \tag{5.2}$$

Noting that $ZL/\nu \sim Re$ this yields

$$1 : \frac{1}{Re}. \tag{5.3}$$

So, from this very crude argument, the theory is expected to hold for $Re \gg 1$. In practice, one finds that the conditions for a similarity decay law are much less stringent than, say, the conditions for the Kolmogorov $-5/3$ slope (von Kármán & Lin 1949). In the simulations shown here, the lowest value of Reynolds number is

around 50, $Re \sim 50$. Therefore, in the worst case scenario, the neglected terms are approximately 50 times smaller than the retained terms in (2.14). It is clear from the results that this level of smallness for the terms proportional to ν is sufficient to satisfy an approximate similarity decay.

However, we can infer the effect of Reynolds number and large-scale eddy strength ($\sim ZL$) by examining results from two simulations, run 3 and run 10. These differ only by Reynolds number with run 10 having the larger Re. From figure 4, run 3 has a higher value of γ^* (i.e., asymptotic $L_\parallel^+/L_\perp^+$). One factor contributing to the different values of γ^* is probably the different grid size in the two simulations. Further, it is known that mean-field-induced anisotropy depends on Reynolds number, so that may play a role here. The ratio L^+/L^-, on the other hand, admits almost equal values for the two runs, presumably since the cross-helicity is the same for both cases. The 'energy' similarity decay constant, α^+, as expected, decreases from run 3 to run 10, due to increased Re (Linkmann *et al.* 2015, 2017; Bandyopadhyay *et al.* 2018*b*). However, the 'length scale' similarity constant, β^+, appears to be less sensitive to Reynolds number.

It is interesting to note that Kármán–Howarth-like similarity decay has been observed in two-dimensional (2-D) MHD (Biskamp & Schwarz 2001). However, a comparison of similarity solutions in 2-D MHD (or two-and-a-half-dimensional, that is, three-component vectors in a two-dimensional plane (2.5-D MHD)) and strong-mean-field 3-D MHD is not entirely straightforward since 2-D MHD also admits an inverse cascade of mean-squared magnetic potential, A. This requires that some magnetic energy is also inverse cascaded and is thus not available for direct cascade to the dissipative small scales. Exploring that parameter space is beyond the scope of the current paper. In particular, the 2-D runs would need to scan E/A (E is the energy) and the 3-D 'comparison' runs would require a scan of B_0, as well as varying the initial polarization (2-D versus '2.5-D').

Further, using 2.5-D fully kinetic particle-in-cell simulations, it has been shown that weakly collisional plasmas support similarity decay (Wu *et al.* 2013; Parashar *et al.* 2015). It will be interesting to extend and test the similarity decay phenomenologies discussed here to three-dimensional kinetic simulations, shear driven flows, compressible plasmas, etc. It is not clear why the quantity $\gamma = L_\parallel/L_\perp$ attains a constant value. Other types of turbulent flow that develop anisotropy, due to rotation, stratification, convection, etc., may also admit a similar stabilization of the ratio of the parallel and perpendicular length scales. Another interesting direction in which the similarity solution can be extended is quasi-static MHD turbulence (see Verma (2017) for a review). We plan to take up these endeavours in the future.

Acknowledgements

This research is supported by NASA under grant NNX17AB79G, and Heliospheric Supporting Research grants 80NSSC18K1210 and 80NSSC18K1648, as well as the Parker Solar Probe Project under Princeton subcontract SUB000016S. The simulations were performed using the Dante and Casella clusters at the University of Delaware, USA.

REFERENCES

BANDYOPADHYAY, R., CHASAPIS, A., CHHIBER, R., PARASHAR, T. N., MATTHAEUS, W. H., SHAY, M. A., MARUCA, B. A., BURCH, J. L., MOORE, T. E., POLLOCK, C. J. *et al.* 2018 Incompressive energy transfer in the earth's magnetosheath: magnetospheric multiscale observations. *Astrophys. J.* **866** (2), 106.

BANDYOPADHYAY, R., OUGHTON, S., WAN, M., MATTHAEUS, W. H., CHHIBER, R. & PARASHAR, T. N. 2018*b* Finite dissipation in anisotropic magnetohydrodynamic turbulence. *Phys. Rev.* X **8**, 041052.

BATCHELOR, G. K. 1953 *The Theory of Homogeneous Turbulence*. Cambridge University Press.

BIGOT, B., GALTIER, S. & POLITANO, H. 2008*a* Development of anisotropy in incompressible magnetohydrodynamic turbulence. *Phys. Rev.* E **78**, 066301.

BIGOT, B., GALTIER, S. & POLITANO, H. 2008*b* Energy decay laws in strongly anisotropic magnetohydrodynamic turbulence. *Phys. Rev. Lett.* **100**, 074502.

BISKAMP, D. & SCHWARZ, E. 2001 On two-dimensional magnetohydrodynamic turbulence. *Phys. Plasmas* **8** (7), 3282–3292.

BREECH, B., MATTHAEUS, W. H., MINNIE, J., BIEBER, J. W., OUGHTON, S., SMITH, C. W. & ISENBERG, P. A. 2008 Turbulence transport throughout the heliosphere. *J. Geophys. Res.* **113** (A8), A08105.

DOBROWOLNY, M., MANGENEY, A. & VELTRI, P. 1980 Fully developed anisotropic hydromagnetic turbulence in interplanetary space. *Phys. Rev. Lett.* **45**, 144–147.

DONZIS, D. A., YEUNG, P. K. & SREENIVASAN, K. R. 2008 Dissipation and enstrophy in isotropic turbulence: resolution effects and scaling in direct numerical simulations. *Phys. Fluids* **20**, 045108.

DRYDEN, H. L. 1943 A review of the statistical theory of turbulence. *Q. Appl. Maths* **1** (1), 7–42.

GHOSH, S., MATTHAEUS, W. H. & MONTGOMERY, D. 1988 The evolution of cross-helicity in driven/dissipative two-dimensional magnetohydrodynamics. *Phys. Fluids* **31** (8), 2171–2184.

GOLDREICH, P. & SRIDHAR, S. 1995 Toward a theory of interstellar turbulence: II. Strong Alfvénic turbulence. *Astrophys. J.* **438**, 763–775.

GRAPPIN, R. 1986 Onset and decay of two-dimensional magnetohydrodynamic turbulence with velocity–magnetic field correlation. *Phys. Fluids* **29**, 2433–2443.

HOSSAIN, M., GRAY, P. C., PONTIUS, D. H. JR., MATTHAEUS, W. H. & OUGHTON, S. 1995 Phenomenology for the decay of energy-containing eddies in homogeneous MHD turbulence. *Phys. Fluids* **7** (11), 2886–2904.

HOSSAIN, M., GRAY, P. C., PONTIUS, D. H. JR., MATTHAEUS, W. H. & OUGHTON, S. 1996 Is the Alfvén-wave propagation effect important for energy decay in homogeneous MHD turbulence? *AIP Conf. Proc.* **382** (1), 358–361.

DE KÁRMÁN, T. & HOWARTH, L. 1938 On the statistical theory of isotropic turbulence. *Proc. R. Soc. Lond.* A **164**, 192–215.

VON KÁRMÁN, T. & LIN, C. C. 1949 On the concept of similarity in the theory of isotropic turbulence. *Rev. Mod. Phys.* **21**, 516–519.

KOLMOGOROV, A. N. 1941 Dissipation of energy in the locally isotropic turbulence. *C. R. Acad. Sci. URSS* **32**, 16 (Reprinted in *Proc. R. Soc. Lond.* A **434**, 15–17 (1991)).

LINKMANN, M., BERERA, A. & GOLDSTRAW, E. E. 2017 Reynolds-number dependence of the dimensionless dissipation rate in homogeneous magnetohydrodynamic turbulence. *Phys. Rev.* E **95**, 013102.

LINKMANN, M. F., BERERA, A., MCCOMB, W. D. & MCKAY, M. E. 2015 Nonuniversality and finite dissipation in decaying magnetohydrodynamic turbulence. *Phys. Rev. Lett.* **114**, 235001.

MATTHAEUS, W. H., GOLDSTEIN, M. L. & MONTGOMERY, D. C. 1983 Turbulent generation of outward-traveling interplanetary Alfvénic fluctuations. *Phys. Rev. Lett.* **51**, 1484–1487.

MATTHAEUS, W. H., GOLDSTEIN, M. L. & ROBERTS, D. A. 1990 Evidence for the presence of quasi-two-dimensional nearly incompressible fluctuations in the solar wind. *J. Geophys. Res.* **95** (A12), 20673–20683.

MATTHAEUS, W. H., ZANK, G. P. & OUGHTON, S. 1996 Phenomenology of hydromagnetic turbulence in a uniformly expanding medium. *J. Plasma Phys.* **56** (3), 659–675.

MONIN, A. S. & YAGLOM, A. M. 1975 *Statistical Fluid Mechanics*, vol. 2. MIT Press.

MONTGOMERY, D. C. 1982 Major disruption, inverse cascades, and the Strauss equations. *Phys. Scr.* **T2/1**, 83–88.

MONTGOMERY, D. C. & TURNER, L. 1981 Anisotropic magnetohydrodynamic turbulence in a strong external magnetic field. *Phys. Fluids* **24**, 825–831.

ONSAGER, L. 1949 Statistical hydrodynamics. *Il Nuovo Cimento* **6**, 279–287.

OUGHTON, S., DMITRUK, P. & MATTHAEUS, W. H. 2004 Reduced magnetohydrodynamics and parallel spectral transfer. *Phys. Plasmas* **11** (5), 2214–2225.

OUGHTON, S. & MATTHAEUS, W. H. 2005 Parallel and perpendicular cascades in solar wind turbulence. *Nonlinear Process. Geophys.* **12** (2), 299–310.

OUGHTON, S., MATTHAEUS, W. H., SMITH, C. W., BREECH, B. & ISENBERG, P. A. 2011 Transport of solar wind fluctuations: a two-component model. *J. Geophys. Res.* **116**, A08105.

OUGHTON, S., PRIEST, E. R. & MATTHAEUS, W. H. 1994 The influence of a mean magnetic field on three-dimensional magnetohydrodynamic turbulence. *J. Fluid Mech.* **280**, 95–117.

OUGHTON, S., WAN, M., SERVIDIO, S. & MATTHAEUS, W. H. 2013 On the origin of anisotropy in magnetohydrodynamic turbulence: the role of higher-order correlations. *Astrophys. J.* **768**, 10.

PARASHAR, T. N., MATTHAEUS, W. H., SHAY, M. A. & WAN, M. 2015 Transition from kinetic to MHD behavior in a collisionless plasma. *Astrophys. J.* **811** (2), 112.

POLITANO, H., GOMEZ, T. & POUQUET, A. 2003 von Kármán–Howarth relationship for helical magnetohydrodynamic flows. *Phys. Rev.* E **68**, 026315.

POLITANO, H. & POUQUET, A. 1998*a* Dynamical length scales for turbulent magnetized flows. *Geophys. Res. Lett.* **25** (3), 273–276.

POLITANO, H. & POUQUET, A. 1998*b* von Kármán–Howarth equation for magnetohydrodynamics and its consequences on third-order longitudinal structure and correlation functions. *Phys. Rev.* E **57**, R21–R24.

ROBINSON, D. C. & RUSBRIDGE, M. G. 1971 Structure of turbulence in the zeta plasma. *Phys. Fluids* **14**, 2499–2511.

SHEBALIN, J. V., MATTHAEUS, W. H. & MONTGOMERY, D. 1983 Anisotropy in MHD turbulence due to a mean magnetic field. *J. Plasma Phys.* **29** (3), 525–547.

TAYLOR, G. I. 1938 The spectrum of turbulence. *Proc. R. Soc. Lond.* A **164**, 476–490.

TEACA, B., VERMA, M. K., KNAEPEN, B. & CARATI, D. 2009 Energy transfer in anisotropic magnetohydrodynamic turbulence. *Phys. Rev.* E **79**, 046312.

USMANOV, A. V., GOLDSTEIN, M. L. & MATTHAEUS, W. H. 2014 Three-fluid, three-dimensional magnetohydrodynamic solar wind model with eddy viscosity and turbulent resistivity. *Astrophys. J.* **788** (1), 43.

VERMA, M. K. 2017 Anisotropy in quasi-static magnetohydrodynamic turbulence. *Rep. Prog. Phys.* **80** (8), 087001.

WAN, M., OUGHTON, S., SERVIDIO, S. & MATTHAEUS, W. H. 2010 On the accuracy of simulations of turbulence. *Phys. Plasmas* **17** (8), 082308.

WAN, M., OUGHTON, S., SERVIDIO, S. & MATTHAEUS, W. H. 2012 von Kármán self-preservation hypothesis for magnetohydrodynamic turbulence and its consequences for universality. *J. Fluid Mech.* **697**, 296–315.

WU, P., WAN, M., MATTHAEUS, W. H., SHAY, M. A. & SWISDAK, M. 2013 von Kármán energy decay and heating of protons and electrons in a kinetic turbulent plasma. *Phys. Rev. Lett.* **111**, 121105.

ZANK, G. P., MATTHAEUS, W. H. & SMITH, C. W. 1996 Evolution of turbulent magnetic fluctuation power with heliocentric distance. *J. Geophys. Res.* **101**, 17093–17107.